

Correlation effects in the triangular lattice single-band system Li_xNbO_2

K.-W. Lee,^{1,*} J. Kuneš,^{2,3} R. T. Scalettar,¹ and W. E. Pickett¹

¹*Department of Physics, University of California, Davis, California 95616, USA*

²*Theoretical Physics III, Center for Electronic Correlations and Magnetism, Institute of Physics, University of Augsburg, Augsburg 86135, Germany*

³*Institute of Physics, Academy of Sciences, Cukrovarnická 10, CZ-162 53 Prague 6, Czech Republic*

(Received 31 July 2007; published 25 October 2007)

Superconductivity in hole-doped Li_xNbO_2 has been reported with $T_c \approx 5$ K in the range $0.45 \leq x < 0.8$. The electronic structure is based on a two-dimensional triangular Nb lattice. The strong trigonal crystal field results in a single Nb d_{z^2} band isolated within a wide gap, leading to a single-band triangular lattice system. The isolated, partially filled band has a width $W=1.5$ eV with dominant *second* neighbor hopping. To identify possible correlation effects, we apply dynamical mean field theory and quantum Monte Carlo (QMC) using on-site Coulomb repulsion $U=0-3$ eV and check selected results using determinant QMC. For U as small as 1 eV, the single particle spectrum displays a robust lower Hubbard band, suggesting the importance of correlation effects in Li_xNbO_2 even for $U \leq W$. At half-filling ($x=0$), a Mott transition occurs at $U_c \approx 1.5$ eV. Coupling between the $O A_g$ phonon displacement and correlation effects is assessed.

DOI: 10.1103/PhysRevB.76.144513

PACS number(s): 71.20.Be, 71.20.Dg, 71.27.+a, 74.25.Jb

I. INTRODUCTION

Not long after the discovery of high temperature superconductivity in layered cuprate compounds, Geselbracht *et al.* discovered superconductivity at $x=0.45$ and 0.50 in the layered niobate Li_xNbO_2 with $T_c \approx 5$ K.¹ Samples were obtained by removing Li (hence electrons) from band insulating LiNbO_2 . This superconductivity has been confirmed in the range $0.45 \leq x \leq 0.79$ with T_c showing no significant dependence on Li concentration,¹⁻⁴ but no superconductivity in the weakly doped range between $x=0.84$ and $x=1$.³ Hall effect measurements confirmed hole-type carriers,⁵ consistent with LiNbO_2 being a band insulator. The difficulty in synthesizing materials with $x < 0.45$ may be related to the considerable covalency of Li along the c direction that is reflected in the Born effective charge.^{6,7}

Recently, Liu *et al.* revisited the superconductor ($x=0.68$) using specific heat measurements.⁴ The electronic specific heat can be fitted well using the BCS-type s -wave symmetry pairing. Additionally, the linear specific heat coefficient $\gamma_{exp}=3.59$ mJ/mol K² and the Debye temperature 462 K were obtained. The virtual crystal approximation (Li nuclear charge $Z=2+x$) leads to the band structure value $\gamma_b=2.425$ mJ/mol K² at $x=0.68$, corresponding to weak electron-phonon coupling strength $\lambda = \frac{\gamma_{exp}}{\gamma_b} - 1 \approx 0.48$, which could, however, be enough to account for $T_c \approx 5$ K. The electron-phonon mechanism is consistent with stated theoretical viewpoints.^{6,8}

There are two interesting sister materials. An isostructural and isovalent Na_xNbO_2 has been observed to be superconducting with a little lower $T_c \approx 4$ K, in the range $0.5 \leq x \leq 0.7$.^{9,10} Interpreted as an isotope shift, $\alpha = -d(\ln T_c)/d(\ln M)$ (M =mass) is 0.27. This value might be thought to imply phonon-mediated pairing, but the important coupling is not expected to be to the Li (Na) ion. Another system is H_xLiNbO_2 , showing superconductivity with $T_c = 5$ K at $x=0.3$ and 0.5 .¹¹ Due to lack of structure studies as well as doping studies, the mechanism and what role H plays are not yet resolved.

In the $\mathcal{M}(\text{S,Se})_2$ system with a transition metal \mathcal{M} , competition between a charge density wave (CDW) transition and superconductivity is frequently observed. Recently, Morosan *et al.* synthesized Cu_xTiSe_2 .¹² By intercalating Cu (i.e., electron donation from Cu), the CDW is suppressed and this system becomes superconducting with the maximum $T_c \approx 4$ K at $x=0.08$. The Wilson ratio $R \sim 0.35$ is small, implying the importance of correlation effects. Another compound for comparison is Na_xCoO_2 , which becomes a superconductor at $x \sim 1/3$ by intercalating water. Also, the dehydrated compound displays an interesting phase diagram with unique insulating phase at $x=0.5$ and shows large correlation effects. As intensively studied by some of the present authors,¹³ correlation effects in this system lead to charge disproportionation on the Co sublattice.

In addition to the common layered structure, both $\mathcal{M}(\text{S,Se})_2$ and Cu_xTiSe_2 have an edge-sharing octahedral framework, similar with NbO_6 trigonal prismatic coordination in Li_xNbO_2 . These similarities imply the significance of correlation effects in this niobate. At $x=0$ (NbO_2), Nb has only one valence electron ($4d^1$) and the possibility of a Mott transition naturally arises. The observed structure of NbO_2 is distorted rutile,¹⁴ and the layered form may not be accessible experimentally.

In this paper, we investigate correlation effects on the presumed Mott insulating and nonstoichiometric phases using the dynamical mean field theory (DMFT) approximation.¹⁵ Selected results are compared with determinant quantum Monte Carlo calculations, where intersite correlations are included and the only limitations are the lattice size and the temperature. For varying strength of repulsion (whose value is not known), and for fillings $n=1, 4/3$, and $5/3$ (note $n=x+1$), we obtain the spectral density, and at $n=1$, we identify the critical strength for a metal-insulator transition and display the evolution of system characteristics through the transition. Finally, we present changes in the spectral density due to (frozen) A_g phonon displacements.

The triangular lattice aspect itself has assumed renewed interest, due in part to the discovery of superconductivity in

the Na_xCoO_2 system. The nearest-neighbor triangular Hubbard model has been studied to uncover how it differs from the square lattice that is used as a model of the high temperature superconductors; its nonbipartite nature is found to be important in frustrating local spin correlations. We will compare results for Li_xNbO_2 where second neighbor coupling dominates, to the same dynamical mean field approximation calculations for the nearest-neighbor case of Aryanpour *et al.*¹⁶

II. STRUCTURE AND CALCULATION

LiNbO_2 is based on a double-layered hexagonal structure ($P6_3/mmc$, No. 194) with lattice parameters $a=2.90 \text{ \AA}$ and $c=10.46 \text{ \AA}$.^{2,3,17-20} Li and Nb atoms lie on $2a$ sites $(0,0,0)$ and $2d$ sites $(\frac{2}{3}, \frac{1}{3}, \frac{1}{4})$, respectively. O atoms occupy $4f$ sites $(\frac{1}{3}, \frac{2}{3}, z)$. In this material, NbO_6 units place the Nb ion in trigonal prismatic coordination. The O internal parameter z , which is measured from the Li layers, shows some disagreement between reports, and our calculations use the experimental value $z=0.1263$ (Ref. 18) for which the electronic structure was analyzed earlier.⁶ This value leads to Nb-O bond length 2.116 \AA and O-Nb-O bond angles 86.5° and 75.4° .

We have carried out first principles, local density approximation (LDA) calculations using the full-potential local-orbital code (FPLO),²¹ and the results are consistent with previous reports.^{6,7} The basis set was Li $(1s)2s2p3d$, Nb $(4s4p)5s5p4d$, and O $2s2p3d$. (The orbitals in parentheses indicate semicore orbitals.) As reported previously,^{6,8} the electronic structure shows strong two dimensionality, and for our investigation of correlation effects, we neglect the k_z dispersion. Our DMFT calculations were carried with two-dimensional tight-binding (TB) parameters $t_1=64 \text{ meV}$, $t_2=100 \text{ meV}$, and $t_3=33 \text{ meV}$, leading to bandwidth $W=1.5 \text{ eV}$. These hopping parameters were obtained using Wannier function techniques.⁶ The TB band structure and density of states (DOS) are displayed in Fig. 1.

Studies of lithium deintercalation in the range $0.5 \leq x \leq 1$ by Kumada *et al.* display negligible change in the structure parameters including Nb-O bond length.¹⁷ This behavior is consistent with the observation that the electronic structure follows a rigid band model well.^{6,8,20} Thus, these tight-binding parameters will be used for all x . (Since another structure¹⁴ is observed, $2H\text{-NbO}_2$ as considered here would be at best a metastable state.)

Hirsch-Fye quantum Monte Carlo (QMC) DMFT calculations¹⁵ were carried out to investigate dynamic correlation effects, applying the on-site Coulomb repulsion U less than 3 eV to the single isolated d_{z^2} Wannier function. The DMFT study is based on the Hubbard model

$$H = \sum_{i,j,\sigma} t_{ij}(c_{i\sigma}^\dagger c_{j\sigma} + c_{j\sigma}^\dagger c_{i\sigma}) - \mu \sum_{i\sigma} n_{i\sigma} + U \sum_i n_{i\uparrow} n_{i\downarrow}, \quad (1)$$

with the hopping parameters t_{ij} between sites i and j , the chemical potential μ , the spin quantum number σ , $c_{j\sigma}^\dagger$ creates an electron of spin σ at site j , and $n_{i\sigma} \equiv c_{i\sigma}^\dagger c_{i\sigma}$ is the number operator. The results reported here are for $T=1100 \text{ K}$ (i.e., 0.1 eV). 40–100 time slices are used for the QMC runs.

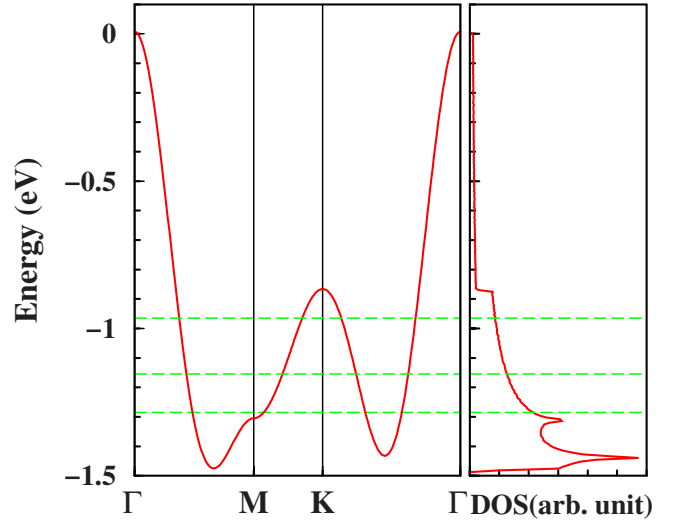


FIG. 1. (Color online) Two-dimensional tight-binding band structure and density of states, using up to third neighbor hopping parameters ($t_1=64 \text{ meV}$, $t_2=100 \text{ meV}$, and $t_3=33 \text{ meV}$), for the single isolated d_{z^2} state in LiNbO_2 . The dashed horizontal lines indicate the Fermi energy E_F in the rigid band picture for electron fillings $n=1$, $4/3$, and $5/3$ from bottom to top. The centroid of the band E_0 lies on 18 meV below E_F for $n=4/3$. Note that the lower half of weight is localized within 0.2 eV width, only 13% of the total bandwidth.

The spectral density $A(\omega)$ has been obtained using the maximum-entropy (MaxEnt) analytic continuation technique developed by Jarrell and Gubernatis.²² In MaxEnt, good QMC data, close to Gaussian distribution, are crucial. We checked the statistics up to 12×10^6 sweeps and also about $500 k$ points in the two-dimensional irreducible wedge. However, at small and large U regimes, the spectral densities, especially near $\omega=0$, depend noticeably on the convergence parameters. In this paper we will show the results in range of $U=0.5\text{--}2.5 \text{ eV}$, which shows robust results for $A(\omega)$. MaxEnt can be performed in a few different ways. In our calculations, both classic and Bryan techniques have been used and show consistent results. The other ingredient in MaxEnt is the default model for the spectral density.²² Since the default model is immaterial for good data, two different ways based on a Gaussian model were tried. One is independently calculated using the same default model for each U , and the other way is that a converged result for previous higher U value is used as a default model for next small U . These methods give consistent results, indicating the robustness of results from the MaxEnt technique.

The bulk of our results have been obtained with this DMFT approach. To assess whether intersite correlations may affect our conclusions, we complement them with a limited set of simulations using determinant quantum Monte Carlo (DQMC),²³ performed for the same Hamiltonian [Eq. (1)] but on finite spatial lattices. This approach includes the momentum dependence of the self-energy, but has the drawback of not working in the thermodynamic limit, as DMFT does. As in the DMFT QMC solver, DQMC requires a discretization of the inverse temperature β . We have chosen the interval $\Delta\tau=0.5$ which satisfies the condition $t_i U (\Delta\tau)^2 \ll 1$

required for the ‘‘Trotter errors’’ associated with the discretization to be small. Our runs typically used 2000 sweeps to equilibrate the lattice and 20 000 sweeps to take measurements. We have looked at the density and short-range spin correlations on 12×12 lattices in addition to the 9×9 lattice results shown here, and observe only minor changes.

III. METAL-INSULATOR TRANSITION

A. Electron filling versus chemical potential

We first address the metal-insulator transition (MIT) at half-filling. When a gap exists, the occupied electron density remains unchanged for values of the chemical potential μ within the gap. This behavior can be observed as a plateau in electron filling $n(\mu)$ plots as U is increased, and is displayed in the top panel of Fig. 2. Since there is a Hartree-Fock-like shift of the entire spectrum with U for the form of Hamiltonian we use, the chemical potential is shifted simply by $U/2$ and denoted by μ^* . Already at $U=1$ eV, an inflection is clear near half-filling. This inflection point becomes a plateau of ~ 0.1 eV width at $U=1.5$ eV, indicating proximity to the MIT.

The critical coupling strength U_c for the MIT can be determined more precisely using two different methods. First, choosing $\mu^*=0.05$ eV (chosen somewhat above $\mu^*=0$ for clarity), the filling approaches unity as $U \rightarrow 1.5$ eV, as shown in inset of Fig. 2 (top panel). Second, and most clearly, vanishing compressibility $\kappa=dn/d\mu$ signifies the onset of the insulating phase. The bottom panel of Fig. 2 shows that κ is reduced by an order of magnitude for $U=1.5$ eV, but only truly vanishes for U close to 2 eV. It must be recalled, however, that the calculations are done at $T=0.1$ eV, and temperature broadening is $\sim \pi T$ in addition to other temperature effects, so requiring κ to vanish overestimates U_c . Considering the $n(\mu^*)$ plot in the inset of Fig. 2, we identify $U_c \approx 1.5$ eV as the (low temperature) critical strength.

Figure 3 shows the intersite spin correlations $\langle S_i^+ S_j^- \rangle$, obtained with DQMC on a 9×9 lattice. Two temperatures are shown, $T=1100$ K and $T=750$ K. The dominant tendency is toward antiferromagnetic orientation between second neighbor spins connected by t_2 , which is certainly reasonable given that it is the largest hopping, and hence has the largest value of $J=4t^2/U$. This short-range order increases strongly as T is lowered, and the asymmetry around half-filling becomes sharp and more pronounced. Near-neighbor spins, connected by t_1 , have a correlation which is almost an order of magnitude smaller, and its increase with lowering temperature is less pronounced. This small near-neighbor correlation is strongly dependent on band filling, being ferromagnetic for $n < 1$ and antiferromagnetic for $n > 1$. Interestingly, while the third neighbor spins connected by t_3 are essentially uncorrelated, spins which are separated linearly by three lattice constants (fifth neighbors), for which there is no direct hopping, exhibit significant antiferromagnetic correlations for $n < 1$ and ferromagnetic correlations for $n > 1$, i.e., *opposite* in sign to the near-neighbor correlation. Overall, the local spin order is markedly different on the two sides of half-filling, $n=1$, in contrast to the square lattice (and bipartite

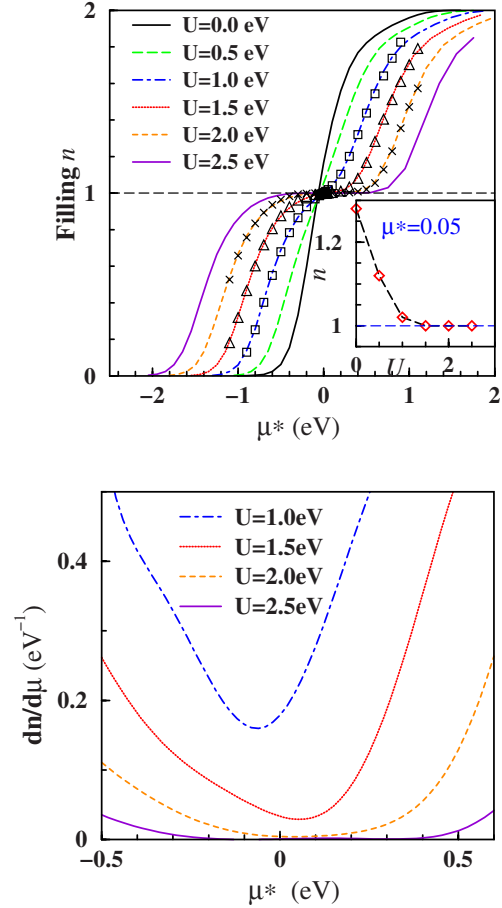


FIG. 2. (Color online) Top: Electron filling n versus effective chemical potential $\mu^* = \mu - U/2$, when changing the on-site Coulomb repulsion U . The lines and symbols are the results of DMFT and DQMC calculations, respectively. The excellent agreement is partly a consequence of the magnetic frustration of the triangular lattice which diminishes the importance of including intersite correlations (see text). Even for $U=1.0$ eV, the slope changes significantly near half-filling, which is indicated by the dashed horizontal line. Above $U=1.5$ eV, there is a plateau at half-filling. Inset: n vs U plot at $\mu^*=0.05$, which displays clearly a metal-to-insulator transition completing ($n \rightarrow 1$) near $U=1.5$ eV. Bottom: Compressibility $\kappa = dn/d\mu$ versus μ^* near the critical U regime, showing more clearly where it approaches zero and finally becomes vanishingly small.

lattices generally) where the order is symmetric about half-filling.

Coupling to second neighbors alone (as occurs here, crudely speaking) separates the triangular lattice into three independent triangular sublattices, each with lattice constant $\sqrt{3}a$. On each sublattice, there are ‘‘near-neighbor’’ antiferromagnetic correlations, which are frustrated on the triangular lattice. Near-neighbor hopping couples a given site to three sites of each of the other sublattices, and antiferromagnetic nearest neighbor coupling tends to add to the frustration. Third neighbor hopping also connects to three sites of each of the other two sublattices, although the sites are far enough apart that any additional frustration is probably not an issue. This picture leads perhaps to even stronger frustration than on the simple triangular lattice and rationalizes why the re-

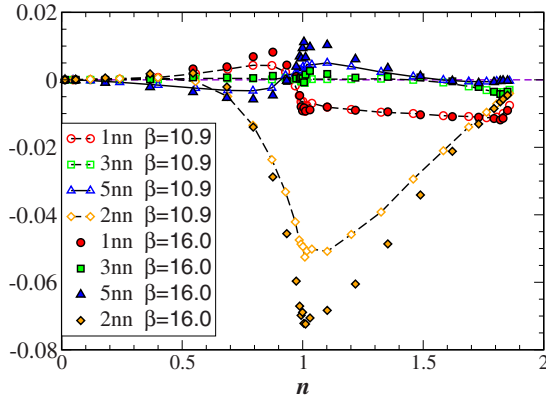


FIG. 3. (Color online) Determinant QMC result for the spin-spin correlation function for temperatures of 1100 K ($\beta=10.9$) and 750 K ($\beta=16$), versus band filling n . $U=1$, and energies are in eV. The fifth neighbor (5nn) is the third neighbor along a straight line from the reference site.

sults for $n(\mu)$ and the compressibility (and perhaps other properties) are so similar in DQMC and in DMFT (which neglects intersite correlations).

B. U -dependent spectral density at half-filling

At half-filling, the MIT can also be observed through the evolution of $A(\omega)$, shown in Fig. 4. For $U=1$ eV, the spectral density has clearly begun splitting into two parts, the lower (LHB) and upper (UHB) Hubbard bands. At $U=1.5$ eV, a gap has opened, consistent with the identification above of $U_c \approx 1.5$ eV. The gap increases monotonically with U for stronger coupling, as expected. No peak is seen at the chemical potential as the gap opens because of the relatively high temperature used here (roughly three times higher than used by Aryanpour *et al.*¹⁶ for the case of near-neighbor hopping only).

This spectral density shows two interesting features. First, this gap opening occurs simultaneously with the appearance of a low-binding-energy peak just below $\omega=0$. Second, recall that within LDA ($U=0$), half of the weight lies in the

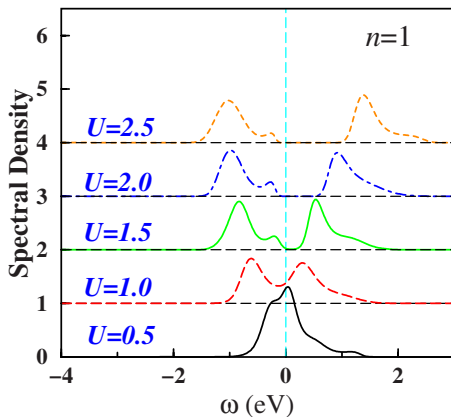


FIG. 4. (Color online) Effect of the on-site Coulomb repulsion U (in units of eV) on spectral density, which is obtained from MaxEnt, for $n=1$. At $U=1.5$ eV, a gap opens clearly.

lower 13% of the total bandwidth (see Fig. 1), but that at half-filling equal weight goes to the LHB and UHB. The band asymmetry fades fairly rapidly as U increases, with a remnant peak on the low-binding-energy side of the LHB and the high-binding-energy tail on the UHB, reflecting the structure in the underlying $U=0$ density of states (again, see Fig. 1).

In single-band near-neighbor models with a single hopping t , the correlation strength is gauged in terms of the ratio of U/W with an unambiguous bandwidth W . However, in the triangular lattice, the tight-binding DOS has a long high energy tail and steep lower edge, as shown in Fig. 1. This extremely asymmetric shape suggests that W alone does not give a meaningful measure of the DOS. We define an effective bandwidth \tilde{W} in terms of the second moment of the DOS. From $\tilde{W} \approx 0.60$ eV, we obtain a critical Coulomb interaction strength ratio $U_c/\tilde{W} \approx 2.5$ for the metal-to-insulator transition.

Using DMFT(QMC), Aryanpour *et al.* investigated the half-filled triangular lattice¹⁶ with only nearest-neighbor hopping ($t=-1$ in arbitrary units) for which $\tilde{W} \approx 4.9$ (the full bandwidth is $W=9|t|=9$). They obtained $U_c=12 \pm 0.5$ eV at a temperature of 400 K, or $U_c/\tilde{W} \approx 2.5-2.6$, the same as for Li_xNbO_2 ($x=0$) above (carried out at 1160 K). Thus, in this case, the more complex dispersion and altered DOS shape have negligible effect on the critical interaction strength ratio.

C. Local susceptibility at half-filling

At half-filling, the local moment $m_{rms} = \sqrt{\langle m_z^2 \rangle} \equiv \sqrt{\langle (n_\uparrow - n_\downarrow)^2 \rangle}$ increases from $\frac{1}{\sqrt{2}}$ at $U=0$ to unity for $U \rightarrow \infty$. For the half-filled system $n=1$, $m_{rms} = \sqrt{1-2d}$, where d is the fraction of doubly occupied sites. The imaginary time correlation function of the local moment $\chi(\tau) = \langle m(\tau)m(0) \rangle$ contains additional information about how the moment decorrelates in imaginary time from its value $\chi(\tau=0) = \langle m_z^2 \rangle$. As shown in Fig. 5, as τ increases in the range $[0, \beta/2]$, $\chi(\tau)$ decreases strongly when U is small, whereas for $U > U_c$, $\chi(\tau)$ becomes nearly flat.

The bottom panel of Fig. 5 shows the local susceptibility $\chi_{loc} \equiv (1/\beta) \int_0^\beta \chi(\tau) d\tau$ versus U . When U surpasses U_c , the local susceptibility rapidly saturates. The variance σ of $\chi(\tau)$ from its average value (χ_{loc}) is also displayed in Fig. 5. $\sigma(U)$ drops by roughly a factor of 40 between $U=0$ and $U=3$ eV, having its maximum (negative) slope around $U=1$.

IV. NONSTOICHIOMETRIC PHASE

In this section, we will address the hole-doped phases, specifically two fillings $n=4/3$ ($\text{Li}_{1/3}\text{NbO}_2$, representing the regime not yet synthesized) and $n=5/3$ ($\text{Li}_{2/3}\text{NbO}_2$, representing the reported superconducting regime) through spectral density studies. Comparison of these results with experimental data will enable the identification of the strength of correlation effects.

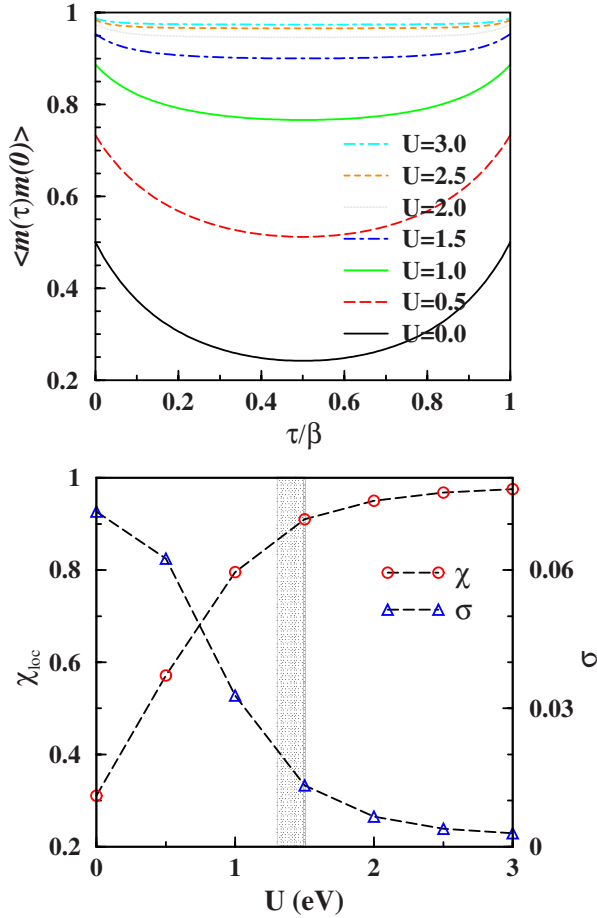


FIG. 5. (Color online) Top: Change in the correlation function $\langle m(\tau)m(0) \rangle$ of local moment m as U increases. Bottom: U -dependent local susceptibility χ_{loc} (left) and standard deviation σ (right) over $(0, \beta)$ for the correlation function. The σ plot shows that variance of the correlation function is strongly reduced by the transition to the insulating phase.

A. Correlation effects on spectral density

Figure 6 shows $A(\omega)$ for $n=4/3$ and $5/3$. At $n=4/3$, even for $U=1.0$ eV, a robust LHB is established. By $U=1.5$ eV $=U_c$, the LHB completely separates from the more intense peak at -0.15 eV. The LHB is clearly identifiable and contains about 0.3 electron per spin, which is close to the number of holes per spin, $n_h=1/3$. The structure around the chemical potential and around 0.5 eV is persistent as U increases, but is not monotonic and may not be above the resolution of the MaxEnt technique that is used to obtain these spectral densities. Certainly, there is no obvious upper Hubbard band that shifts monotonically with U .

At $n=5/3$, the LHB appears for U as small as 0.5 eV. Its weight is near 0.1 per spin independent of U and shifts downward almost linearly with U ; the hole-doping level is $n_h=0.17/\text{spin}$. For the main spectral weight peak around -0.5 eV and in the electron-addition spectrum, there is little change as U increases. The LHB can be understood simply. In a snapshot of a doped system, one would see doubly occupied sites and singly occupied sites (for substantial U). The process corresponding to the LHB is removing an elec-

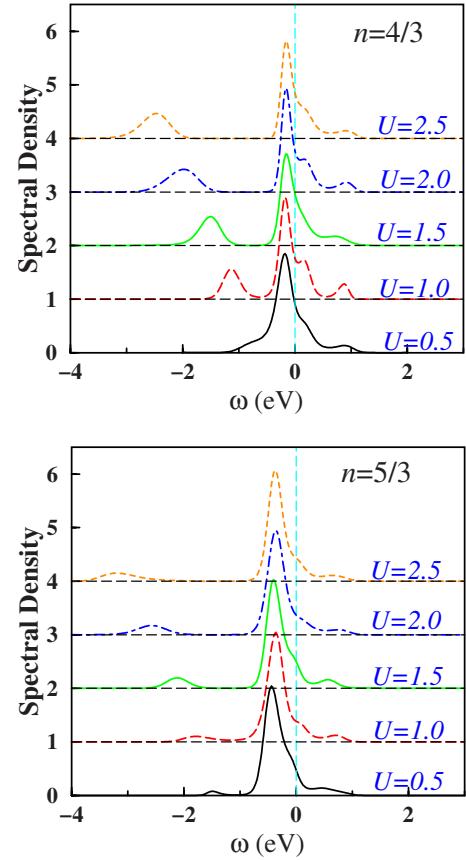


FIG. 6. (Color online) Effect of the on-site Coulomb repulsion U (in units of eV) on spectral densities, which are obtained from MaxEnt, for $n=4/3$ (top) and $5/3$ (bottom). As expected from the bandwidth, correlated behavior already appears at $U=0.5$ eV. (For details, see text.) Note that the spectral densities are normalized, i.e., $\int A(\omega)d\omega=1$.

tron from the singly occupied sites, so the fraction of such sites is equal to the number of holes, and thus similar to the weight of the LHB. This picture seems to be more precise for the higher hole concentration ($n=4/3$).

Cherkashenko *et al.* reported²⁰ the x-ray emission spectrum for Nb $4d \rightarrow 2p$ transitions for Li_xNbO_2 , $x=0.97$ and 0.71 , i.e., for the near band insulator and superconducting compositions, respectively. With their low resolution, all that could be identified was a decrease in the occupied Nb $4d$ intensity and some narrowing, without measurable shift in the peak, as the Li concentration was reduced. This behavior is roughly consistent with a rigid band picture, if the narrowing can be ascribed to the Fermi level moving from the top of the band (insulating phase) down into the band (metallic phase). However, the edge position did not change as it would in a rigid band picture, so the interpretation is not certain. Higher resolution x-ray measurements, compared with our predictions, will be very useful in identifying correlation effects in this system.

B. Effect of Nb–O bond stretching mode

The calculations of Ylvisaker and Pickett in the band insulating phase led to a rough scale for the deformation po-

TABLE I. Change in direct width W , effective width \tilde{W} (see text for the definition), and critical U_c for MIT (in units of eV) when O is displaced. See the caption of Fig. 7 for the definition of the displacements d_+ and d_- . The centroid of the band E_0 (in meV) is measured from the value of E_F for $n=4/3$. There is a consistent critical strength $U_c/\tilde{W} \approx 2.5$. Each tight-binding parameters (in meV) used here are from Ref. 6. The compared DOSs are shown in the top panel of Fig. 7.

	Tight binding			W	\tilde{W}	E_0	U_c
	t_1	t_2	t_3				
d_+	19	102	10	1.1	0.51	-48	1.2
d_0	64	100	33	1.5	0.60	-18	1.5
d_-	122	94	56	2.0	0.80	-77	1.7

tential $\mathcal{D} = dW/dz \sim 2.5 \text{ eV}/\text{\AA}$ (half the bandwidth change per unit displacement), which is a substantial value that suggests the importance of O displacement Δz for electron-phonon coupling, i.e., transport and superconductivity.⁶ To investigate effects of the O A_g phonon mode on $A(\omega)$, we have used O ion displacements $\Delta z = \pm 0.10 \text{ \AA}$ along the c direction. This displacement is representative of the maximum amplitude of the A_g mode, and it happens to be similar to the variation of the S position in NbS_2 reported between $x=0$ and $x=0.67$ in isovalent, isostructural, and superconducting Li_xNbS_2 .^{24,25} This magnitude of displacement leads to significant changes in hopping integrals, as reproduced in Table I, resulting in considerably different DOS shape for each O position.

The DOS (obtained from the tight-binding fit, but equivalent to the first principles result) displayed in the top panel of Fig. 7 shows that the most significant change is in bandwidth, about $\pm 0.5 \text{ eV}$ for $\mp 0.10 \text{ \AA}$ change in O position, giving the mean deformation potential mentioned above. The variation of the DOS is not well characterized simply by W , however, because although W increases, the portion of the DOS containing $\sim 60\text{--}70\%$ of the states narrows by roughly a factor of 2. As a result, the position of E_F and DOS at $E_F N(E_F)$ change significantly for all fillings. This effect is especially operative at $n=5/3$ filling: the shifting of E_F across the Van Hove singularity reflects the fact that there is a transfer of charge (holes, in this case) between the low mass hole pocket at Γ and the higher mass hole pocket at the two K points. Since the bandwidth W seems to change more than other identifiable energy structures, the scale $\mathcal{D} = 2.5 \text{ eV}/\text{\AA}$ mentioned above is probably an overestimate of actual deformation potentials at the Fermi surface. The fact that O displacement makes the Fermi level shift across a Van Hove singularity indicates that nonadiabatic processes are involved in the neighborhood of $n=5/3$, i.e., in the reported superconducting regime. Similar nonadiabatic effects were identified²⁶ in MgB_2 and have not yet been treated properly.

Considering correlation effects within our DMFT approach, O displacement affects $A(\omega)$ most strongly within $\pm 0.5 \text{ eV}$ of the chemical potential, as shown in the bottom panel of Fig. 7. The LHB is hardly affected, either in position or in weight. The spectral densities that are displayed are for $U=2 \text{ eV}$, but for all U studied here the phonon effects are

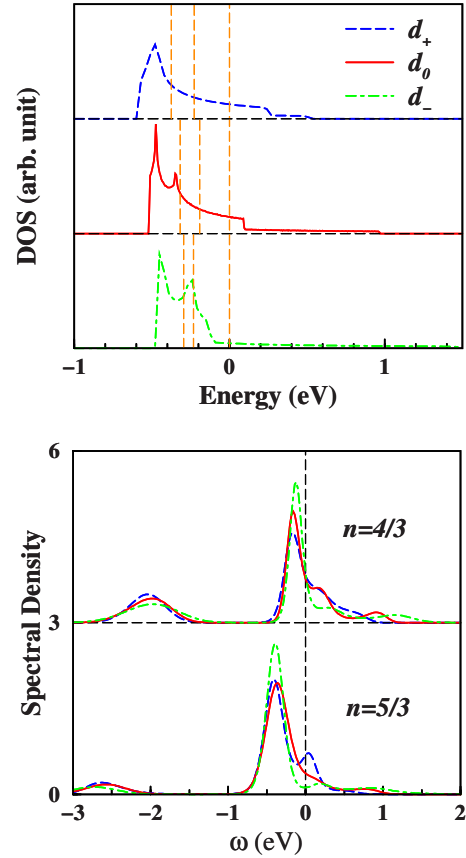


FIG. 7. (Color online) Effect of O displacement on spectral densities. O is displaced by $\pm 0.10 \text{ \AA}$ in the $\langle 001 \rangle$ direction. d_0 is the optimized position. d_- and d_+ denote contraction and elongation of the Nb–O bond length, respectively. Top: Tight-binding DOS (i.e., $U=0$) for the O displacement. The densities of states are aligned with respect to E_F for $n=5/3$, set to zero. For each case, the dashed vertical lines denote E_F for $n=1, 4/3$, and $5/3$ (left to right). Bottom: Change in spectral densities, which shows effects of the phonon mode, at $U=2 \text{ eV}$. The line designations are the same as in the top panel.

similar. At $n=5/3$, which is in the range of observed superconductivity, $A(\omega=0)$ [the interacting analog of $N(E_F)$] fluctuates strongly, while at $n=4/3$, $A(\omega=0)$ varies little. The changes occur for ω only up to a few tenths of eV. The stronger changes for $n=5/3$ may arise from the already very strong change in the underlying $N(E_F)$ (see the top panel of Fig. 7).

V. SUMMARY

The single d_{z^2} band in Li_xNbO_2 , isolated due to large trigonal crystal field splitting, requires three neighbor hopping parameters to reproduce its dispersion, second neighbor hopping being dominant. This long range of hybridization reflects the fact that the corresponding Wannier function is not well localized, having significant O $2p$ and neighboring Nb $4d$ character in addition to the on-site $4d_{z^2}$ part. The dispersion leads to highly asymmetric DOS which contains half its weight in the lower 13% of bandwidth.

Using DMFT(QMC), we have investigated correlation effects on the spectral densities and have followed the Mott transition using both the compressibility and the spectral density. At half-filling, a metal-to-insulator transition occurs at $U_c \approx 1.5$ eV. Because of long tail and steep edge of DOS in the two-dimensional tight-banding model for the triangular lattice, however, we have introduced an effective bandwidth \tilde{W} obtained from the second moment of the density of states to characterize the band. The critical interaction strength ratio $U_c/\tilde{W} \sim 2.5$ for the Mott transition is the same as was obtained for the triangular lattice nearest-neighbor Hubbard model, indicating that the more complex dispersion does not affect the position of the metal-insulator transition in this system.

Calculation of the spin correlation functions with determinant QMC verifies that second neighbor correlations are by far the largest, as expected from the hopping parameters. Spin correlations between other neighbors are very minor. We find, however, that the behavior of the band filling $n(\mu)$ and the compressibility are virtually identical in DMFT (which neglects intersite spin correlations) and DQMC, justifying *a posteriori* our use of DMFT for this triangular lattice system. The dominant second neighbor hopping t_2 tends

to partition the lattice into three weakly coupled triangular sublattices (lattice constant $\sqrt{3}$); each of these is frustrated with the antiferromagnetic coupling, and the small coupling between these sublattices adds to the frustration.

The spectral density was used to assess the strength and character of correlation effects in Li_xNbO_2 , both for the static lattice and for frozen displacements of the O A_g phonon. These results were presented for a grid of interaction (U) strengths, since the appropriate value for Li_xNbO_2 is not yet known. These results will be useful in the interpretation of high-resolution photoemission data, which are needed to further our understanding of this very interesting triangular lattice superconductor.

ACKNOWLEDGMENTS

We acknowledge J. L. Luo for clarifying his specific heat measurements and K. Aryanpour, S. Chiesa, and E. R. Ylvisaker for useful discussions. This work was supported by DOE Grant No. DE-FG03-01ER45876, by Stewardship Science Academic Alliance Program (DOE) Grant No. DE-FG01-06NA26204, and by DOE's Computational Materials Science Network.

*Current address: Department of Display and Semiconductor Physics, Korea University, Jochiwon, Chungnam 339-700, South Korea

- ¹M. J. Geselbracht, T. J. Richardson, and A. M. Stacy, *Nature* (London) **345**, 324 (1990).
- ²P. Bordet, E. Moshopoulou, S. Liesert, and J. J. Capponi, *Physica C* **235-240**, 745 (1994).
- ³E. G. Moshopoulou, P. Bordet, and J. J. Capponi, *Phys. Rev. B* **59**, 9590 (1999).
- ⁴G. T. Liu, J. L. Luo, Z. Li, Y. Q. Guo, N. L. Wang, D. Jin, and T. Xiang, *Phys. Rev. B* **74**, 012504 (2006).
- ⁵D. G. Kellerman, G. P. Shveikin, A. P. Tyutyunnik, V. G. Zubkov, V. A. Perelyaev, T. V. D'yachkova, N. I. Kadyrova, A. S. Fedukov, S. A. Turzhevskii, V. A. Gubanov, G. P. Shveikin, A. E. Kafkin, and V. I. Voronin, *Supercond., Phys. Chem. Technol.* **5**, 2035 (1992).
- ⁶E. R. Ylvisaker and W. E. Pickett, *Phys. Rev. B* **74**, 075104 (2006).
- ⁷E. R. Ylvisaker, K.-W. Lee, and W. E. Pickett, *Physica B* **383**, 63 (2006).
- ⁸D. L. Novikov, V. A. Gubanov, V. G. Zubkov, and A. J. Freeman, *Phys. Rev. B* **49**, 15830 (1994).
- ⁹D. G. Kellerman, V. G. Zubkov, A. P. Tyutyunnik, V. S. Gorshkov, V. A. Perelyaev, G. P. Shveikin, S. A. Turzhevskii, V. A. Gubanov, and A. E. Kafkin, *Supercond., Phys. Chem. Technol.* **5**, 966 (1992).
- ¹⁰A. P. Tyutyunnik, V. G. Zubkov, D. G. Kellerman, V. A. Perelyaev, A. E. Kafkin, and G. Svensson, *Eur. J. Solid State Inorg. Chem.* **33**, 53 (1996).
- ¹¹N. Kumada, S. Watauchi, I. Tanaka, and N. Kinomura, *Mater. Res. Bull.* **35**, 1743 (2000).
- ¹²E. Morosan, H. W. Zandbergen, B. S. Dennis, J. W. G. Bos, Y. Onose, T. Klimczuk, A. P. Ramirez, N. P. Ong, and R. J. Cava,

Nat. Phys. **2**, 544 (2006).

- ¹³K.-W. Lee, J. Kuneš, and W. E. Pickett, *Phys. Rev. B* **70**, 045104 (2004); K.-W. Lee, J. Kuneš, P. Novak, and W. E. Pickett, *Phys. Rev. Lett.* **94**, 026403 (2005); K.-W. Lee and W. E. Pickett, *ibid.* **96**, 096403 (2006).
- ¹⁴V. Eyert, *Europhys. Lett.* **58**, 851 (2002), references therein.
- ¹⁵For review, see A. Georges, G. Kotliar, W. Krauth, and M. J. Rozenberg, *Rev. Mod. Phys.* **68**, 13 (1996); G. Kotliar, S. Y. Savrasov, K. Haule, V. S. Oudovenko, P. Parcollet, and C. A. Marianetti, *ibid.* **78**, 865 (2006).
- ¹⁶K. Aryanpour, W. E. Pickett, and R. T. Scalettar, *Phys. Rev. B* **74**, 085117 (2006).
- ¹⁷N. Kumada, S. Muramatu, F. Muto, N. Kinomura, S. Kikkawa, and M. Koizumi, *J. Solid State Chem.* **73**, 33 (1988).
- ¹⁸G. Meyer and R. Hoppe, *Angew. Chem., Int. Ed. Engl.* **13**, 744 (1974); *J. Less-Common Met.* **46**, 55 (1976).
- ¹⁹M. J. Geselbracht, A. M. Stacy, A. R. Garcia, B. G. Silbernagel, and G. H. Kwei, *J. Phys. Chem.* **97**, 7102 (1993).
- ²⁰V. M. Cherkashenko, M. A. Korotin, V. I. Anisimov, V. V. Shumilov, V. R. Galakhov, D. G. Kellerman, V. G. Zubkov, and E. Z. Kurmaev, *Z. Phys. B: Condens. Matter* **93**, 417 (1994).
- ²¹K. Koepernik and H. Eschrig, *Phys. Rev. B* **59**, 1743 (1999).
- ²²M. Jarrell and J. E. Gubernatis, *Phys. Rep.* **269**, 133 (1996).
- ²³R. Blankenbecler, D. J. Scalapino, and R. L. Sugar, *Phys. Rev. D* **24**, 2278 (1981).
- ²⁴P. A. Salyer, M. G. Barker, A. J. Blake, D. H. Gregory, and C. Wilson, *Acta Crystallogr., Sect. C: Cryst. Struct. Commun.* **C59**, i4 (2003).
- ²⁵F. Jellinek, G. Brauer, and H. Müller, *Nature* (London) **185**, 376 (1960).
- ²⁶L. Boeri, G. B. Bachelet, E. Cappelluti, and L. Pietronero, *Phys. Rev. B* **65**, 214501 (2002).